batteries

MDPI

Article

Calorimetric Studies on Chemically Delithiated $LiNi_{0.4}Mn_{0.4}Co_{0.2}O_2$: Investigation of Phase Transition, Gas Evolution and Enthalpy of Formation

Wenjiao Zhao [1,*], Julian Gebauer [2], Thomas Bergfeldt [2], Magnus Rohde [2], Carlos Ziebert [2], Yong Du [3] and Hans J. Seifert [2,*]

1 Volkswagen AG, 38239 Salzgitter, Germany
2 Karlsruhe Institute of Technology, Institute of Applied Materials-Applied Materials Physics (IAM-AWP), 76344 Eggenstein-Leopoldshafen, Germany
3 State Key Lab of Powder Metallurgy, Central South University, Changsha 410083, China; yong-du@csu.edu.cn
* Correspondence: wenjiao.zhao@volkswagen.de (W.Z.); hans.seifert@kit.edu (H.J.S.)

Abstract: $Li_{1.11}(Ni_{0.4}Mn_{0.4}Co_{0.2})O_2$ powders were chemically delithiated by $(NH_4)_2S_2O_8$ oxidizer to obtain $Li_x(Ni_{0.4}Mn_{0.4}Co_{0.2})O_2$ powders. The thermal behavior of two delithiated specimens, $Li_{0.76}Ni_{0.41}Mn_{0.42}Co_{0.17}O_{2.10}$ and $Li_{0.48}Ni_{0.38}Mn_{0.46}Co_{0.16}O_{2.07}$, was studied compared to the pristine specimen. Phase transitions at elevated temperatures were investigated by simultaneous thermal analysis (STA) and the gas evolution accompanying the phase transitions was analyzed by mass spectroscopy and an oxygen detector. The enthalpy of two delithiated samples and a pristine specimen were measured by a high temperature drop solution calorimeter. Based on these results, the enthalpies of formation were calculated.

Keywords: chemical delithiation; phase transition; gas evolution; thermal behavior; enthalpy of formation; NMC

check for updates

Citation: Zhao, W.; Gebauer, J.; Bergfeldt, T.; Rohde, M.; Ziebert, C.; Du, Y.; Seifert, H.J. Calorimetric Studies on Chemically Delithiated $LiNi_{0.4}Mn_{0.4}Co_{0.2}O_2$: Investigation of Phase Transition, Gas Evolution and Enthalpy of Formation. *Batteries* **2023**, *9*, 275. https://doi.org/10.3390/batteries9050275

Academic Editor: Sylvain Franger

Received: 28 February 2023
Revised: 24 April 2023
Accepted: 12 May 2023
Published: 17 May 2023

Copyright: © 2023 by the authors. Licensee MDPI, Basel, Switzerland. This article is an open access article distributed under the terms and conditions of the Creative Commons Attribution (CC BY) license (https://creativecommons.org/licenses/by/4.0/).

1. Introduction

Among the key parameters of Li ion batteries—namely power, lifetime, and cost—safety is also important and remains the main challenge for their application [1,2]. The layered Li(Ni, Mn, Co)O_2 (NMC) is widely commercially applied as a positive electrode material, due to its high energy density and good rate performance [3,4]. However, when the Li ion cell is fully charged, the delithiated NMC can be thermally unstable. In its delithiated state, phase transitions are prone to take place at elevated temperatures, accompanied with gas evolution [5–7]. The electrochemical performance and safety are deteriorated by storage or operation at high temperatures. Therefore, a detailed understanding of the thermal behavior and phase transitions of delithiated NMC materials is essential to improve the thermal stability.

The method of chemical delithiation is often used [8–10] for the synthesis of pure delithiated active cathode materials, which avoids the interaction with binder and carbon black in composite cathode electrode. Since the assembly and later disassembly of a cell can be avoided, there is also no contact/reaction between cathode electrode and liquid electrolyte which could introduce reaction products. Additionally, the amount of delithiated sample is not limited by disassembly of cells. Zheng et al. [8] investigated chemically delithiated NMC samples by ab initio computation and experimental methods. Tian et al. [9] studied the thermal behavior of NMC-622 under a delithiated status by surface-sensitive techniques, revealing the chemical and structural characteristics of the bulk and surface of NMC particles after heating. Ma et al. [10] investigated the thermal stability of NMC with different Co contents. NMC samples were chemically delithiated by five kinds of acids to achieve a range of lithium content. With increasing Co content in NMC, a better thermal stability of the delithiated sample was exhibited.

In this work, we attempted to obtain the delithiated positive electrode active material (NMC442) via chemical delithiation using $(NH_4)_2S_2O_8$ as an oxidizer. Medium- and high degree delithiated specimens were prepared with two different Li contents. The thermal behavior of the delithiated specimens was investigated by using simultaneous thermal analysis (STA) combined with mass spectroscopy (MS) and an oxygen detector. The enthalpy was measured by a high temperature oxide melt drop solution calorimeter (Alexsys-1000). Enthalpies of formation from oxides and elements of delithiated and pristine materials are calculated.

2. Experimental

The investigated $Li_{1.11}(Ni_{0.42}Mn_{0.41}Co_{0.17})O_2$ (NMC442) powders and the oxidizer powder $(NH_4)_2S_2O_8$ were purchased from MTI (MTI Coop., Richmond, CA, USA) and Alfa Aesar (Thermo Fisher Scientific, Kandel, Germany), respectively (Table 1). $(NH_4)_2S_2O_8$ powders were dissolved in distilled water, preparing 0.5 mol/L oxidizing solvent. In order to obtain medium- and high degree delithiated specimens, two pristine specimens with a mass of 1 g were immersed in 250 mL and 500 mL oxidizing solvent with a concentration of 0.5 mol/L. After 65 h and 96 h reactions, the delithiated specimens Li_xNMC442 were washed with distilled water three times and filtered. Finally, the samples were dried in a vacuum oven at 120 °C for 24 h. One medium degree delithiated (65 h and 250 mL solvent) and one high degree delithiated specimen (96 h and 500 mL solvent) were obtained.

Table 1. Chemical specification: commercial NMC442 positive electrode materials and oxidizer powder $(NH_4)_2S_2O_8$.

Raw Material	Chemical Formula	Source	Initial Mass Fraction Purity
Lithium nickel manganese cobalt oxide	$Li_{1.11}Ni_{0.42}Mn_{0.41}Co_{0.17}O_2$	MTI	0.9776
Ammoniumpersulfat	$(NH_4)_2S_2O_8$	Alfa Aesar	0.98

The compositions of the delithiated samples were quantitatively determined by inductively coupled plasma with optical emission spectroscopy (ICP-OES) and carrier gas hot extraction (CGHE) measurements. Approximately 5 mg solid specimen was dissolved in 6 mL hydrochloric acid and 2 mL nitric acid at 80 °C for four hours. To measure the contents of transition metal elements (TM: Ni, Co, and Mn) and lithium, the chemical digestion solution was diluted and, thereafter, an internal standard solution was added. For each element analysis, a calibration curve was adopted, which was determined by four selected concentrations. The calibration was conducted within one decade. Two to three different wavelengths of each element have been used for the ICP-OES analysis of the composition. Oxygen contents were determined by CGHE measurements.

The crystal structure of specimens before/after thermal measurements was determined by X-ray diffraction (XRD, Bruker-AXS GmbH, Ettlingen, Germany). The measurements were made in the 2θ angle range of 10–110°, with a step size increment of 0.02. Rietveld profile refinements were carried out using the software Maud 2.67 and Jade 5.

Phase transitions were studied by the combination of simultaneous thermal analysis (STA, NETZSCH, Hanau, Germany), mass spectroscopy (QMS 403C, NETZSCH, Germany), and an oxygen detector (SGM 5T, Zirox GmbH, Greifswald, Germany). Ar gas (purity 99.9999%) with a flow rate of 50 mL/min was used as a protective gas. The produced gases and Ar were collected and investigated by a mass spectrometer (MS) and an oxygen detector. The specimens were heated up to 800 °C with 5 K/min. The masses of pristine, medium, and highly delithiated specimens were 58.62, 56.90, and 59.59 mg, respectively.

The measurements of the enthalpy of the drop solution of pristine and delithiated specimens were performed in a high temperature drop solution calorimeter (Alexsys-1000 calorimeter, Setaram (KEP technologies SA), Caluire-et-Cuire, France). Here, 5–8 mg powder specimens were pressed into pellets with a diameter of 3 mm. The masses of the specimens were carefully controlled to ensure that heat effects were in the range of 5–10 J,

where one drop took approximately 45 min. Between drops, it would take about 1.5 h for the stabilization of the baseline [11]. The specimens were dropped into the right and left cell of the calorimeter alternately from ambient temperature into the molten oxide (sodium molybdate at 701 °C). During the drops Ar gas was introduced as a flushing gas to maintain a constant atmosphere, with a flow rate of 40 mL/min. Moreover, Ar gas was also used to stir the solution to prevent local solvent saturation by bubbling it into the melt with a flow rate of 5 mL/min.

3. Results and Discussion

3.1. ICP-OES and CGHE Results for Pristine and Chemically Delithiated Samples

The results of the ICP-OES measurements are shown in Table 2 for pristine and two delithiated NMC442 materials. TM stands for transition metals. Stoichiometric compositions were calculated based on the assumption that the atomic sum of the transition metals is equal to 1 (TM = 1). The amount of Li per formula unit in medium- and high degree delithiation was 0.76 and 0.48, corresponding to state of charge 50% and 100% of NMC442 cells, respectively. The Li content showed a clear dependence on the degree of delithiation, as it decreased by more than a factor of two from the pristine sample to the high degree delithiated one. The content of the transition metal ions exhibited only small variations upon the degree of delithiation, which can be due to stoichiometric scattering between the samples combined with the level of uncertainty of the analysis method. The same effects can be observed in the molar ratios given in the table. Comparable results were found in a study by Ma et al. [10], in which the delithiation in NMC442 was achieved by applying different acid solutions, adjusting the Li content between x = 1.0 and x = 0.362, respectively.

Table 2. Chemical analysis of the pristine and selected delithiated commercial NMC442 samples. The nominal stoichiometry was calculated based on transition metals' cations equal to 1 in composition (sum TM = 1).

Analyzed Elements		Pristine Specimen	Medium Degree Delithiated Specimen	High Degree Delithiated Specimen
ICP-OES and CGHE wt.%	Li	7.68 ± 0.16	5.33 ± 0.11	3.40 ± 0.07
	Ni	24.40 ± 0.37	24.37 ± 0.37	22.43 ± 0.34
	Mn	22.50 ± 0.41	23.30 ± 0.42	25.90 ± 0.47
	Co	10.10 ± 0.19	10.13 ± 0.19	9.75 ± 0.19
	O	33.60 ± 2.99	34 ± 3.0	33.7 ± 3.0
Molar ratio	Li/sum TM	1.11	0.76	0.48
	Ni/sum TM	0.42	0.41	0.38
	Mn/sum TM	0.41	0.42	0.46
	Co/sum TM	0.17	0.17	0.16
	O/sum TM	2.11	2.10	2.07
Nominal composition		$Li_{1.11}Ni_{0.42}Mn_{0.41}Co_{0.17}O_{2.11}$	$Li_{0.76}Ni_{0.41}Mn_{0.42}Co_{0.17}O_{2.10}$	$Li_{0.48}Ni_{0.38}Mn_{0.46}Co_{0.16}O_{2.07}$

3.2. XRD Results for Pristine and Chemically Delithiated Specimens

The measured XRD patterns of three specimens (pristine, medium-, and high degree delithiated) are shown in Figure 1, and the corresponding results from the Rietveld refinement are listed in Table 3. The initial structure of the pristine sample and main structure of the delithiated specimens are an O3 layered structure (space group $R\bar{3}m$), which belongs to the α-$NaFeO_2$ structure type. However, after delithiation, small shoulders appeared near reflections (003), as shown in Figure 1b,c, which can be assigned to an O1 phase belonging to the trigonal structure $P\bar{3}m1$. Comparing to delithiated NMC442 [10,12], the lattice parameters show a similar decrease. Lattice parameters c remain almost the same in this work, while reference [10,12] show an increased trend for the c parameters. The slight differences could be caused by the implement of different oxidizers for chemical delithiation.

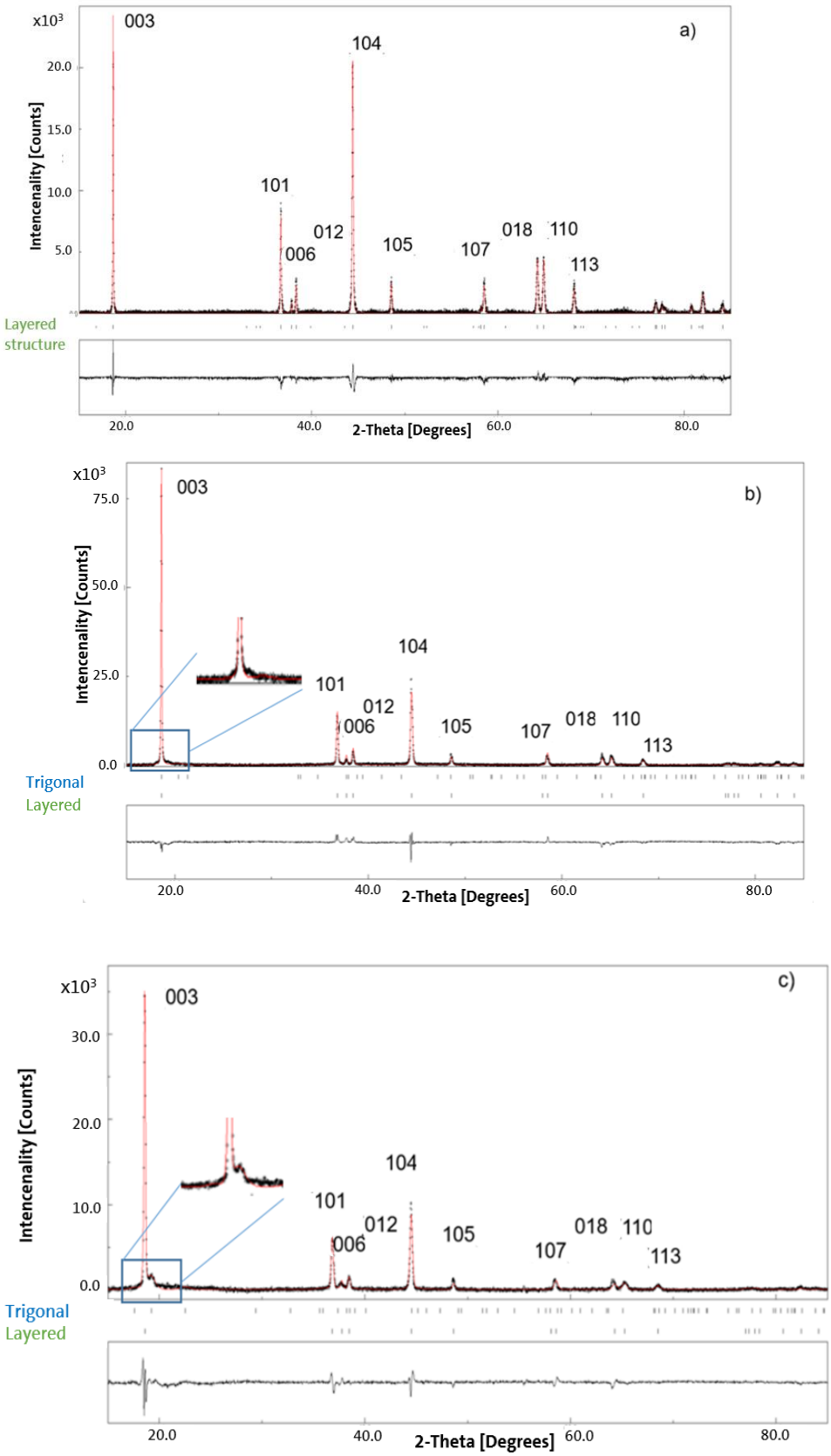

Figure 1. The experimental and calculated XRD patterns of pristine and chemically delithiated commercial $Li_xNMC442$: (**a**) x = 1.11, (**b**) x = 0.76, and (**c**) x = 0.48.

Table 3. Rietveld refinement for X-ray diffraction of the pristine NMC442 and chemically delithiated specimens Li_xNMC442, compared with reference [10,12].

Li Content x	Space Group	Lattice Parameters			Phase wt.%
		a (Å)	*b* (Å)	*c* (Å)	
1.11	$R\bar{3}m$	2.8769 (7)	-	14.2922 (0)	-
0.76	$R\bar{3}m$	2.8606 (8)	-	14.2926 (7)	84.5
0.48	$R\bar{3}m$	2.8562 (2)	-	14.2722 (5)	86.4
1.11	$R\bar{3}m$	2.861		14.238	Ref. [11]
1.04	$R\bar{3}m$	2.865		14.245	
0.97	$R\bar{3}m$	2.870		14.265	
0.90	$R\bar{3}m$	2.874		14.280	
1	$R\bar{3}m$	2.8694 (1)		14.266 (1)	Ref. [12]
0.94	$R\bar{3}m$	2.8616 (3)		14.272 (2)	
0.5	$R\bar{3}m$	2.8280 (5)		14.456 (4)	

The results of the structural analysis of this work can be compared to the studies on the structural and electrochemical behavior of NMC111 [13] and NMC442 [10,12]. The data from X-ray and neutron diffraction on de- and re-intercalated NMC111 by Yin et al. [13] revealed the stability of the rhombohedral $R\bar{3}m$ structure in NMC111 down to a Li content of x < 0.3. Below this Li extraction level, the O1 phase with the trigonal structure $P\bar{3}m1$ appeared.

Additional results were obtained from XRD investigations to determine the phases of the specimens after STA/MS measurement. Figure 2 shows the results of Rietveld refinement: (a) the pristine commercial NMC442 maintained the layered structure. Compared to the commercial NMC442's structure before STA/MS measurement, the coalescence of the (006)/(012) and (018)/(110) reflections indicated an increase in the lattice parameter *a* and a decrease in *c*. The lower intensity ratio of (003)/(104) implied a lower cation mixing after heat treatment up to 800 °C. (b) Three phases, namely a layered structure (space group $R\bar{3}m$), spinel structure (space group $Fd\bar{3}m$), and rock-salt structure (space group $Fm\bar{3}m$), were found to be coexistent in the medium degree delithiated specimen. The previous chemical delithiation probably proceeded as an onion-like model, and the Li ions in core were not extracted, so the layered structure remained qualitatively similar to pristine powders. The intensity of the reflection $(111)_{spinel}$ and $(200)_{rock\text{-}salt}$ reflected the proportion of spinel and rock-salt structures, which were approximately 50% and 46%, respectively. (c) For the deep delithiated sample, spinel structure, and rock-salt structure were found, and the maximal reflection $(003)_{layered}$ disappeared completely. The reflection $(200)_{rock\text{-}salt}$ has a much higher intensity than $(111)_{spinel}$, indicating that rock-salt phase content increases. The formation of the rock-salt phase is directly proportional to the degree of delithiation, accompanied by release of oxygen.

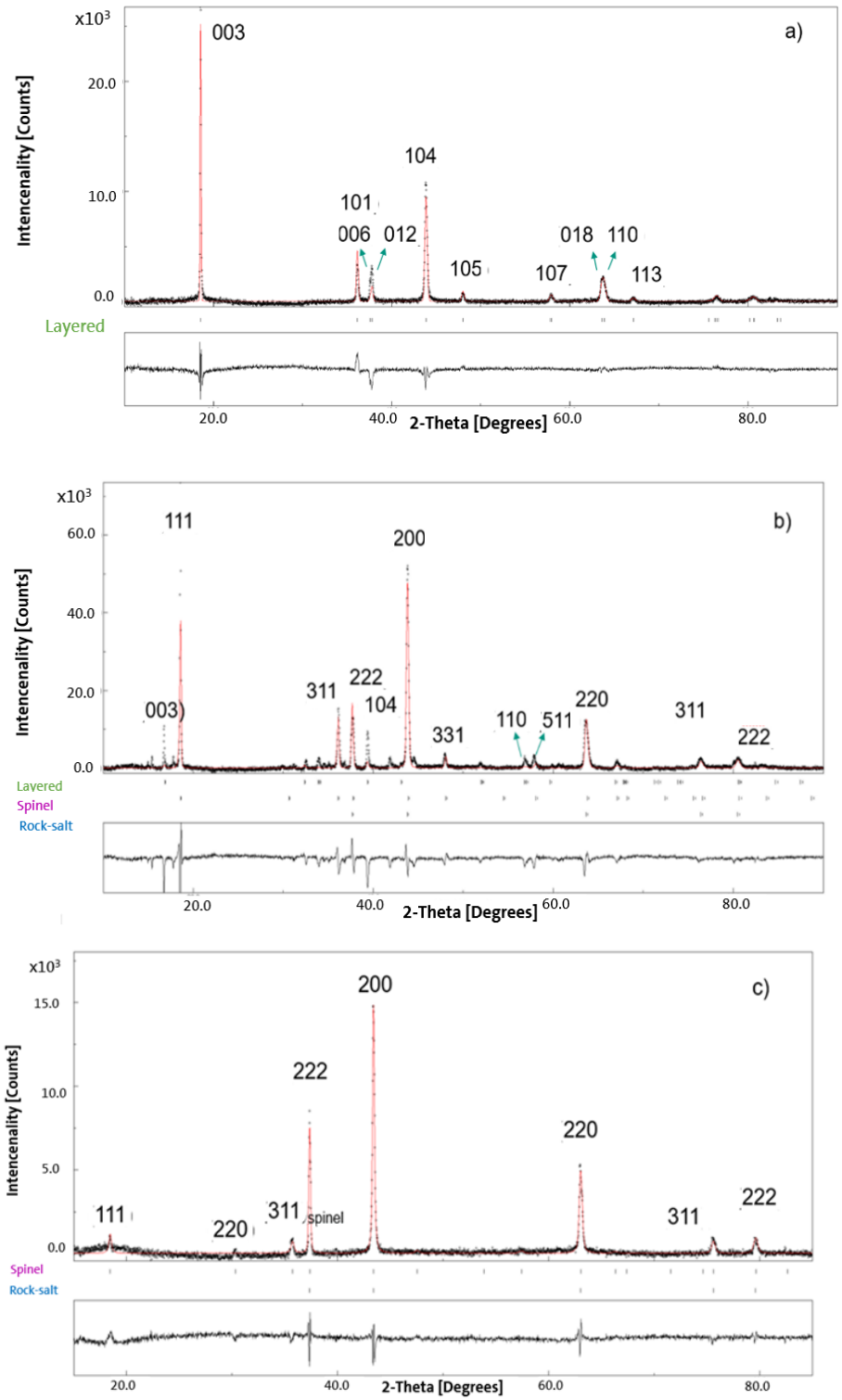

Figure 2. The XRD patterns and Rietveld refinement curves of pristine and chemically delithiated commercial $Li_xNMC442$ after STA/MS measurement with maximum temperature 800 °C (black curve: measured, red curve: refined): (**a**) x = 1.11, (**b**) x = 0.76, and (**c**) x = 0.48.

3.3. Simultaneous Thermal Analysis (STA) and Gas Evolution Study

The heat flow signal and thermogravimetric analysis of the samples with compositions of $Li_{1.11}Ni_{0.42}Mn_{0.41}Co_{0.17}O_{2.11}$, $Li_{0.76}Ni_{0.41}Mn_{0.42}Co_{0.17}O_{2.10}$, and $Li_{0.48}Ni_{0.38}Mn_{0.46}Co_{0.16}O_{2.07}$, respectively, are shown in Figure 3. The mass loss increased significantly with the increasing degree of delithiation. However, the DTA signals (black curves) in Figure 3b,c for materials

with different delithiation degrees are comparable and show similar sequence of multi-reactions. The red curves in Figure 3 are the derivatives of the DTA signal with respect to temperature, which indicate the heat flux changes. As shown in Figure 3a, the temperature derivative of the heat flux signal is flat, indicating no reaction taking place. Compared to the delithiated samples, the pristine sample was thermally stable up to high temperatures with a mass loss of only 0.2%. For the delithiated samples in Figure 3b,c, there were several peaks on the differential heat flux curve. For the medium degree delithiated sample, a sequence of reactions starting above 150 °C extended up to slightly below 700 °C, indicated by DTA peaks. The reactions at 300 °C and above 550 °C, marked the onset of oxygen release, where the phase transitions (Equation (1)) occurred. In Figure 4, the blue curves show oxygen concentration measured by an oxygen detector, and dash black curves are the differential of mass change rate. For the high degree delithiated sample, a comparable sequence of reactions could be observed. The reactions in both delithiated samples were accompanied by a partial mass loss which added up to about 3.5% in the medium delithiated sample and up to 7% in the highly delithiated sample.

The rate of mass change and the O_2 concentration released from the samples as a function of temperature are shown in Figure 4. While the pristine sample showed no significant mass change and oxygen release, strong effects were visible for the delithiated samples. A strong fluctuation in the rate of mass change at around 300 °C triggered the onset of the first release of oxygen, leading to a significant peak in the O_2 concentration which overlapped with a smaller rate of mass change at 400 °C. The onset of a second O_2 concentration peak can be observed above 550 °C. While the sequence of mass change and oxygen release were comparable in both delithiated samples, the effects appear to be more strongly pronounced in the sample with the higher degree of delithiation. The first O_2 concentration peak of the sample with x = 0.48 was nearly doubled compared to the sample with x = 0.76. Furthermore, the oxygen release above 550 °C was strongly broadened and extended to temperatures above 750 °C.

With lower onset temperatures, faster rate of mass change, and larger amount of oxygen released, the delithiated samples show deteriorating thermally stability depending on the degree of delithiation. According to Equation (1) accompanied with further Li loss, this induced a phase transformation from the layered structure to spinel and finally to a rock-salt type phase. The following sequence of phase transitions took place [14] with increasing temperature:

$$\begin{aligned} \mathrm{Li}_x\mathrm{TMO}_2\ \mathrm{layered}(R\bar{3}m) &\xrightarrow{\text{high temperature}} \tfrac{x}{2}\mathrm{Li}_2\mathrm{O} + \mathrm{TM}_3\mathrm{O}_4\ \mathrm{spinel}(Fd\bar{3}m) + \varepsilon\mathrm{O}_2 \\ \mathrm{TM}_3\mathrm{O}_4\ \mathrm{spinel}(Fd\bar{3}m) &\xrightarrow{\text{increasing temperature}} \mathrm{TMO\ rock-salt}(Fm3m) + \varepsilon\mathrm{O}_2 \end{aligned} \tag{1}$$

The gas species released during the temperature rise were measured by the mass spectrometer (MS), and the results are presented as the function of temperature and volume percentage in Figure 5. During the beginning of the heating ramp of the pristine sample, small amounts of nitrogen and oxygen were observed, but both signals disappeared during heating and no further oxygen release could be observed. During the initial heating, the delithiated samples also showed small nitrogen signals. However, on further heating, there were two oxygen peaks detected in both of the delithiated samples. For $Li_{0.76}$NMC442, the first O_2 peak appeared with an onset temperature slightly below 300 °C, while the second peak appeared with an onset between 450 °C and 500 °C. In the $Li_{0.48}$NMC442 sample, the O_2 peaks appeared with a comparable thermal history. Qualitatively, this corresponded to the results of the measurements with the oxygen sensor shown in Figure 4. However, the small shifts in the onset and peak temperatures, respectively, can be explained by differences in the time constants and sensitivities of the two measurement methods.

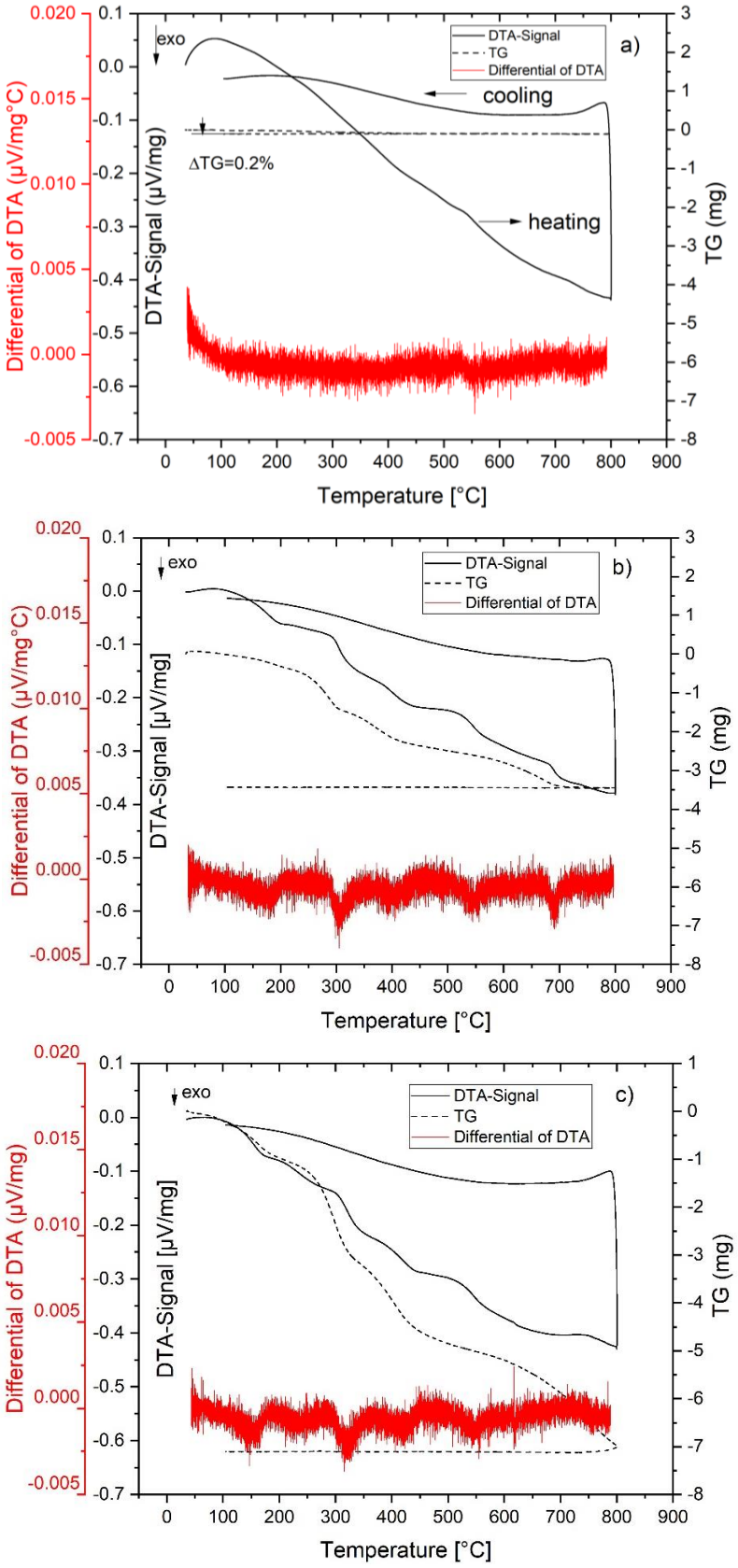

Figure 3. Simultaneous thermal analysis for pristine and chemically delithiated commercial $Li_xNMC442$ samples: (**a**) x = 1.11, (**b**) x = 0.76, and (**c**) x = 0.48.

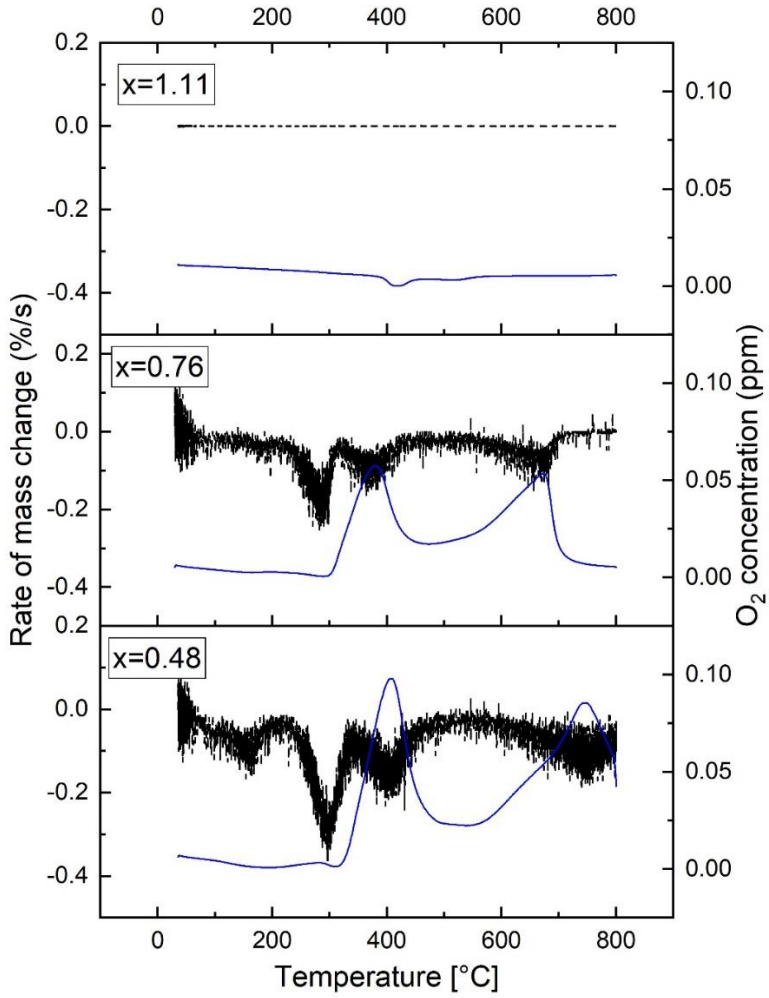

Figure 4. Comparison of selected delithiation degrees by using the first derivative of the mass change percentage with time for commercially available $Li_xNMC442$ samples, regarding the mass loss (black curves) and oxygen concentration (blue curves) measured by an oxygen detector.

Initially Ni^{2+} and Co^{3+} were the electrochemically active ions in the stoichiometric NMC442 positive electrode materials, and their oxidation states in the delithiated samples changed to Ni^{3+}, Ni^{4+}, and Co^{4+}. Upon heating, oxygen vacancies formed in the structure, and the TM cations reduced to lower oxidation states in order to maintain the overall charge neutrality [7]. The thermal stability of the NMC442 materials was significantly affected by the amount of Ni^{3+} and Ni^{4+}, which increased with the degree of delithiation.

3.4. Enthalpy Analysis for Pristine and Chemically Delithiated Samples

The enthalpies of drop solution are listed in Table 4, with the corresponding uncertainties and number of drops. Enthalpies of drop solution are 102.66 ± 1.15 kJ/mol, 99.57 ± 0.95 kJ/mol and 111.27 ± 1.52 kJ/mol for pristine, medium and high degree delithiated specimens, respectively. In Figure 6 the measured heat flow signal (in μV) is shown for the drops of pristine specimens. Masses of dropped specimens are given with corresponding calculated heat effect (in Joule) in parentheses.

Koyama et al. [15] investigated the electronic structure of delithiated NMC (positive cathode material) using first-principles calculations. They reported three oxidation reactions in $Li_{1-x}[Ni_{1/3}Co_{1/3}Mn_{1/3}]O_2$: $0 < x < 1/3$ redox couple $Ni^{2+/3+}$, $1/3 < x < 2/3$ redox couple $Ni^{3+/4+}$, and $2/3 < x < 1$ redox couple $Co^{3+/4+}$. Kim and Chung [16] investigated the same composition and its delithiation procedure. They also reported the oxidation of Ni and Co ions. In contrast to Koyama et al. [15], they reported a $Co^{3+/4+}$ transition for

0 < x < 1. For the Ni oxidation, the experimental results were coincident with Koyama et al.'s calculations. Kim and Chung assumed that differences were caused by investigating particles that were in a non-equilibrious heterogeneous state, whereas Koyama et al. [15] assumed an equilibrious homogeneous state for the calculations.

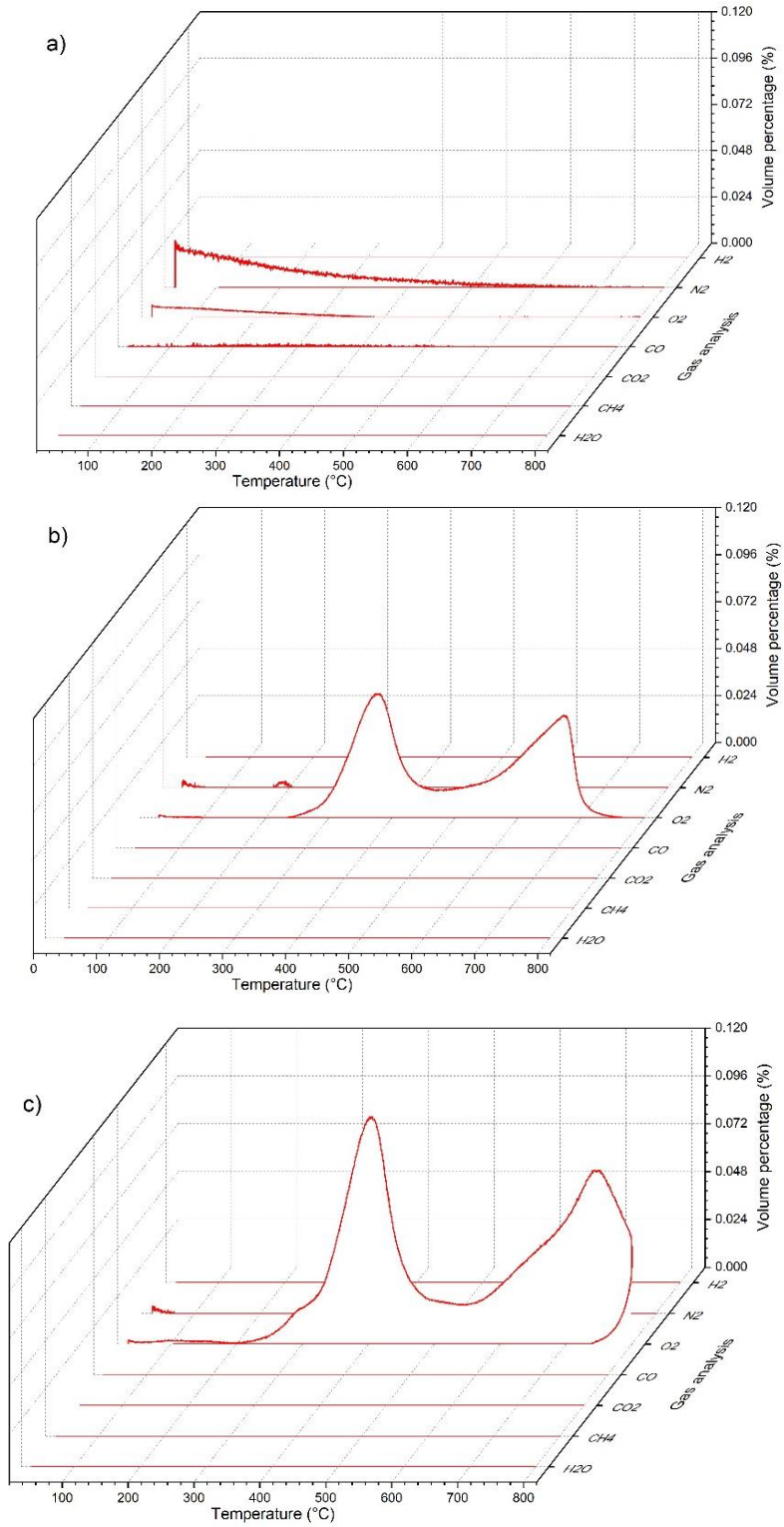

Figure 5. Mass spectroscopy analysis for pristine and chemically delithiated commercial $Li_xNMC442$ samples: (**a**) x = 1.11, (**b**) x = 0.76, and (**c**) x = 0.48.

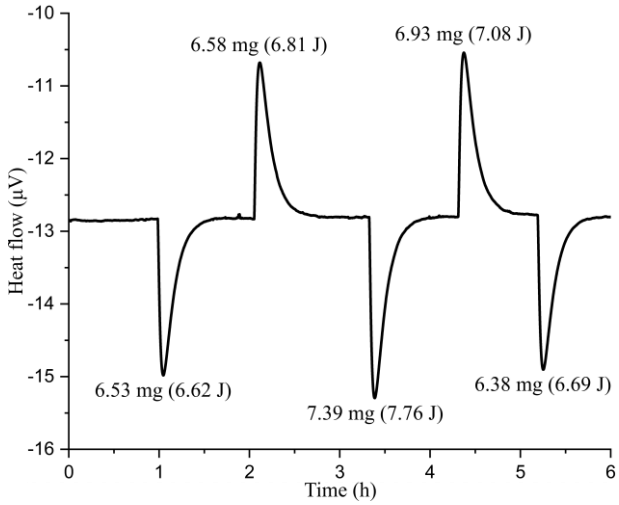

Figure 6. High temperature drop solution experiment on the pristine specimen.

Qiao et al. [17] analyzed the redox evolution in $LiNi_{0.5}Mn_{0.3}Co_{0.2}O_2$. Similar to [15,16], the oxidation of both Ni and Co ions was involved while charging up to 4.2 V, and Mn ions remained in the same oxidation status 4+. Further charging up to 4.5 V resulted in Co ion oxidation solely. At 4.5 V, the electrode surface contained approximately 20% of Ni^{2+}.

In this work, the oxidation states of Ni and Co atoms in the pristine NMC442 sample are considered as 2+ and 3+, respectively. In delithiated samples, the oxidation states of Ni are simplified to a mixture of 2+ and 4+. As shown in Figure 7, the thermodynamic cycle for the calculation of the enthalpy of formation is based on binary oxides and oxygen. Since Co_2O_3 (Co^{3+}), CoO_2 (Co^{4+}), Ni_2O_3 (Ni^{3+}), and NiO_2 (Ni^{4+}) are unstable under normal conditions, the parameters of Li_2O (Li^+), NiO (Ni^{2+}), MnO_2 (Mn^{4+}), and CoO (Co^{2+}) are used according to [18,19]. Deviations α, β, γ, and δ from nominal NMC442 composition determined by ICP-OES and CGHE are also included in the thermodynamic cycle. With a thermodynamic cycle, the enthalpy of formation can be calculated from drop solution calorimetry (Equation (2)). A proper cycle (Figure 7) is as follows: Li-NMC (product) at room temperature $\overset{\Delta_{ds}H}{\rightarrow}$ dissolved Li-NMC at 974 K = dissolved binary oxides (educts) at 974 K $\overset{\Delta_{ds}H}{\leftarrow}$ educts at room temperature. As the dissolved state of the educts (in appropriate ratio) and the product is the same, the only remaining unknown to close the circle is the enthalpy of formation of the product at room temperature from the educts. Binary oxides are used to fulfill the composition conditions for Li, Ni, Mn, and Co. In the thermodynamic cycle, the remaining oxygen fraction ε, caused by the oxidation of Ni^{2+} and Co^{2+} ions, is included with an enthalpy increment derived by the integration of the specific heat capacity of oxygen. The oxygen enthalpy increment from room temperature to 974 K is calculated using Gibbs energy, obtained from SGTE data for pure elements [20]. The enthalpy of formation from elements is calculated using the enthalpies of formation of Li-NMC from Equation (2) and of the binary oxides from the literature (Table 4).

For $Li_{1-x}Ni_{0.4}Mn_{0.4}Co_{0.2}O_2$ specimens, the equations for enthalpy of formation from oxides and elements are summarized in Equations (2) and (3), respectively, as follows:

$$\begin{aligned}\Delta_f H^{\theta,oxide}_{Li_{1-x}Ni_{0.4}Mn_{0.4}Co_{0.2}O_2} &= \tfrac{1-x}{2}\bullet\Delta_{ds}H_{(Li_2O)} + 0.4\bullet\Delta_{ds}H_{(NiO)} + 0.4\bullet\Delta_{ds}H_{(MnO_2)} + 0.2\bullet\Delta_{ds}H_{(CoO)} \\ &+ \tfrac{0.1+0.5\bullet x}{2}\int_{298K}^{974K} C_p(O_2)dT - \Delta_{ds}H_{(Li_{1-x}Ni_{0.4}Mn_{0.4}Co_{0.2}O_2)}\end{aligned} \quad (2)$$

$$\Delta_f H^{\theta,elements}_{Li_aNi_bMn_cCo_dO_e} = \Delta_f H^{\theta,oxides}_{Li_aNi_bMn_cCo_dO_e} + \frac{a}{2}\bullet\Delta_f H_{(Li_2O)} + b\bullet\Delta_f H_{(NiO)} + c\bullet\Delta_f H_{(MnO_2)} + d\bullet\Delta_f H_{(CoO)} \quad (3)$$

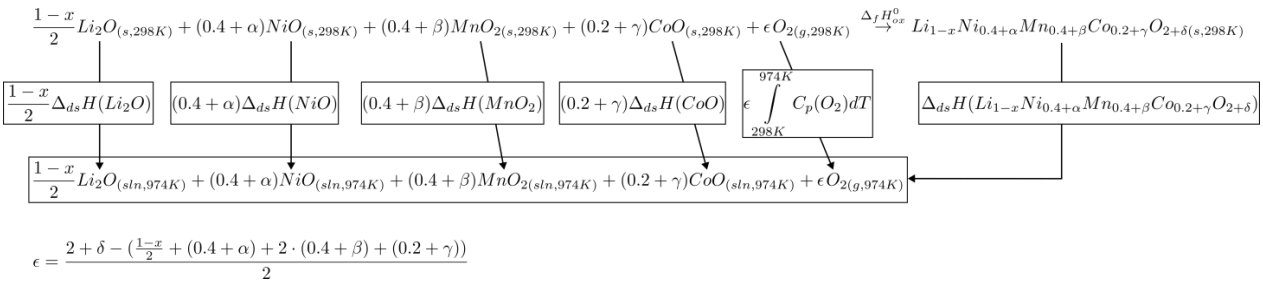

$$\epsilon = \frac{2+\delta-(\frac{1-x}{2}+(0.4+\alpha)+2\cdot(0.4+\beta)+(0.2+\gamma))}{2}$$

Figure 7. Thermodynamic cycle. First line: formation enthalpy of various NMC compositions (with deviations α, β, γ, and δ from nominal NMC442 composition) from binary oxides and oxygen. Second line: enthalpies of drop solution of the oxides. Third line: species in molten solution at 974 K. Last line: equation for oxygen fraction ε.

Assuming x = 0.8 ($Li_{0.2}Ni_{0.4}Mn_{0.4}Co_{0.2}O_2$), Ni^{2+} ions are completely oxidized to Ni^{4+}, leading to $Li^{+}{}_{0.2}Ni^{4+}{}_{0.4}Mn^{4+}{}_{0.4}Co^{3+}{}_{0.2}O^{2-}{}_{2}$. When 0 < x < 0.8, Ni^{4+} will replace Ni^{2+} partially. When x > 0.8, Co^{3+} ions will partially be oxidized to Co^{4+}. According to [19], the enthalpy of formation calculations are based solely on stable binary oxides Li_2O, NiO, MnO_2, and CoO. The change in the oxidation state of Ni and Co is thereby included in the enthalpy of formation from the stable oxides and oxygen. For example, the medium degree delithiated sample $Li_{0.76}Ni_{0.41}Mn_{0.42}Co_{0.17}O_{2.10}$, will be $Li^{+}{}_{0.76}Ni^{4+}{}_{0.12}Ni^{2+}{}_{0.29}Mn^{4+}{}_{0.42}Co^{3+}{}_{0.17}O^{2-}{}_{2.10}$. Equations (4) and (5) are corresponding calculations including the deviations α = 0.01, β = 0.02, γ = −0.03, and δ = 0.1 from nominal Li_1-NMC442 composition determined by ICP-OES and CGHE, as follows:

$$\begin{aligned}\Delta_f H^{\theta,oxide}_{Li_{0.76}Ni_{0.41}Mn_{0.42}Co_{0.17}O_{2.10}} &= \tfrac{0.76}{2}\bullet\Delta_{ds}H_{(Li_2O)} + 0.41\bullet\Delta_{ds}H_{(NiO)} + 0.42\bullet\Delta_{ds}H_{(MnO_2)} + 0.17\bullet\Delta_{ds}H_{(CoO)}\\ &+\left[2.10-\left(\tfrac{0.76}{2}+0.41+0.42\bullet 2+0.17\right)\right]\bullet\tfrac{1}{2}\bullet\int_{298K}^{974K}C_p(O_2)dT\\ &-\Delta_{ds}H_{(Li_{0.76}Ni_{0.41}Mn_{0.42}Co_{0.17}O_{2.10})}\end{aligned} \tag{4}$$

$$\begin{aligned}\Delta_f H^{\theta,oxide}_{Li_{0.76}Ni_{0.41}Mn_{0.42}Co_{0.17}O_{2.10}} &= \tfrac{0.76}{2}\bullet\Delta_{ds}H_{(Li_2O)} + 0.41\bullet\Delta_{ds}H_{(NiO)} + 0.42\bullet\Delta_{ds}H_{(MnO_2)} + 0.17\bullet\Delta_{ds}H_{(CoO)}\\ &+\left[2.10-\left(\tfrac{0.76}{2}+0.41+0.42\bullet 2+0.17\right)\right]\bullet\tfrac{1}{2}\bullet\int_{298K}^{974K}C_p(O_2)dT\\ &-\Delta_{ds}H_{(Li_{0.76}Ni_{0.41}Mn_{0.42}Co_{0.17}O_{2.10})}\end{aligned} \tag{5}$$

The enthalpies of formation from oxides and elements are shown in Figure 8 as a function of the Li content. The results of the present work are in good agreement with the experimental and ab initio calculated results by Masoumi et al. [18]. The further delithiated specimens have less negative enthalpy values, which is considered to be thermodynamically less stable: thermodynamic stability decreases with increasing delithiation.

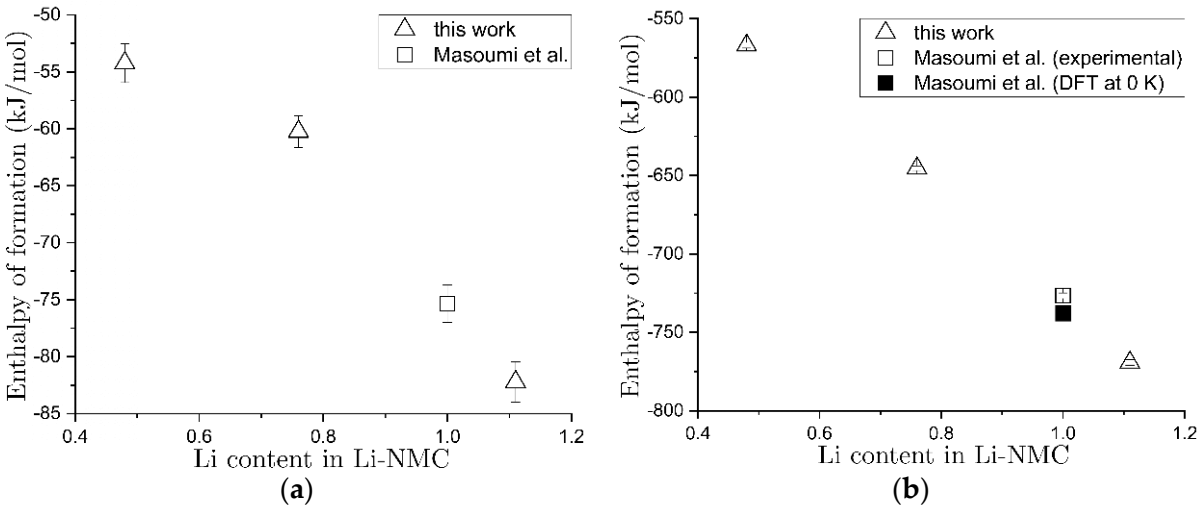

Figure 8. Enthalpy of formation from oxides (**a**) and elements (**b**) versus lithium content, in comparison with experimental and calculated results by Masoumi et al. [18].

Table 4. Enthalpy of drop solution, enthalpy of formation from the oxides, and from the elements of the investigated specimens and of binary oxides from the literature.

Nominal Stoichiometry	Enthalpy of Drop Solution (kJ/mol)	Enthalpy of Formation from Oxides (kJ/mol)	Enthalpy of Formation from Elements (kJ/(mol of Formula)
$Li_{1.11}Ni_{0.42}Mn_{0.41}Co_{0.17}O_{2.11}$	102.66 ± 1.15 (8)	−82.23 ± 1.78	−769.20 ± 1.85
$LiNi_{0.4}Mn_{0.4}Co_{0.2}O_2$	98.86 ± 1.09 (18) [e]	−75.35 ± 1.65 [e]	−726.59 ± 1.72 [e]
$Li_{0.76}Ni_{0.41}Mn_{0.42}Co_{0.17}O_{2.10}$	99.57 ± 0.95 (12)	−60.24 ± 1.39	−645.39 ± 1.47
$Li_{0.48}Ni_{0.38}Mn_{0.46}Co_{0.16}O_{2.07}$	111.27 ± 1.52 (11)	−54.23 ± 1.70	−566.95 ± 1.77
Li_2O	−93.02 ± 2.24 [a,b]		−597.935 ± 0.334 [c]
NiO	35.73 ± 0.95 (8) [a]		−239.743 ± 0.543 [c]
MnO_2	128.92 ± 0.91 (11) [d]		−521.493 ± 0.836 [c]

The uncertainties are given behind the symbol ±, which is two standard deviations from the mean for enthalpy of the drop solution and the propagated uncertainties for enthalpy of formation. The number of experiments is given in parentheses. [a] [19] [b] [21] [c] [22] [d] [23] [e] [18].

4. Conclusions

Different delithiated specimens were obtained by using $(NH_4)_2S_2O_8$ oxidizer via chemical delithiation. The initial rhombohedral phase of the pristine NMC442 sample is stable upon delithiation at room temperature. Phase transitions accompanied with oxygen release were observed during heating in the temperature range from 25 to 800 °C. The onset temperatures of the oxygen concentration peaks indicate the starting of the phase transformations from the layered structure to the spinel and then to the rock-salt structure. Furthermore, a sequence of thermal effects was detected by the STA. Enthalpies of formation from oxides and enthalpies of formation from elements were calculated based on the measured enthalpies of drop solution in sodium molybdate, showing decreasing thermodynamic stabilities with the increasing degree of delithiation with a nearly linear relationship.

Author Contributions: Conceptualization, H.J.S. and Y.D.; methodology, W.Z. and T.B.; software, W.Z.; validation, C.Z., J.G. and M.R.; formal analysis, W.Z., J.G. and M.R.; investigation, W.Z and T.B.; resources, C.Z., T.B. and M.R.; data curation, W.Z.; writing—original draft preparation, W.Z.; writing—review and editing, M.R., C.Z., J.G., T.B., Y.D. and H.J.S.; visualization, W.Z. and J.G.; supervision, C.Z., M.R., Y.D. and H.J.S.; project administration, H.J.S. and Y.D.; funding acquisition, H.J.S. and Y.D. All authors have read and agreed to the published version of the manuscript.

Funding: This research was funded by the German Research Foundation (DFG) under the Project ID 390874152 (POLiS Cluster of Excellence). W.Z. received additional funding from the Helmholtz Association through the Young Investigator Group and partially from the Sino-German Center for Research Promotion in Beijing.

Informed Consent Statement: The research was released in Wenjiao Zhao's doctoral thesis; however, the enthalpy in Table 4 and Figure 8 was recalculated in this paper.

Data Availability Statement: The data presented in this study are available on request from the corresponding author.

Acknowledgments: The authors gratefully acknowledge the technical support of C. Gebert and also the support of M. Steinbrück from the materials chemistry group at IAM-AWP for interpretation of the mass spectroscopy analysis. This work contributes to the research performed at CELEST (Center of Electrochemical Energy Storage Ulm-Karlsruhe).

Conflicts of Interest: The authors declare no conflict of interest. The funders had no role in the design of the study; in the collection, analyses, or interpretation of data; in the writing of the manuscript; or in the decision to publish the results.

References

1. Wu, X.; Song, K.; Zhang, X.; Hu, N.; Li, L.; Li, W.; Zhang, L.; Zhang, H. Safety issues in Lithium ion batteries: Materials and cell design. *Front. Energy Res.* **2019**, *7*, 65. [CrossRef]
2. Chombo, P.; Laoonal, Y. A review of safety strategies of a Li ion battery. *J. Power Sources* **2020**, *478*, 228649. [CrossRef]
3. Rozier, P.; Tarascon, J.M. Review—Li-rich layered oxide cathodes for next-generation Li-ion batteries: Chances and challenges. *J. Electrochem. Soc.* **2015**, *162*, A2490–A2499. [CrossRef]
4. Li, W.; Erickson, E.; Manthiram, A. High-Nickel layered oxide cathodes for Lithium-based automotive batteries. *Nat. Energy* **2020**, *5*, 26–34. [CrossRef]
5. Tian, C.; Lin, F.; Doeff, M. Electrochemical characteristics of layered transition metal oxide cathode materials for lithium ion batteries: Surface, bulk behavior, and thermal properties. *Acc. Chem. Res.* **2018**, *51*, 89–96. [CrossRef]
6. Kasnatscheev, J.; Röser, S.; Börner, M.; Winter, M. Do increased Ni contents in $LiNi_xMn_yCo_zO_2$ (NMC) electrodes decrease structural and thermal stability of Li ion batteries? A thorough look by consideration of the Li+ extraction ratio. *ACS Appl. Energy Mater.* **2019**, *2*, 7733–7737. [CrossRef]
7. Bak, S.; Hu, E.; Zhou, Y.; Yu, X.; Senanayake, S.; Cho, S.; Kim, K.; Chung, K.; Yang, X.; Nam, K. Structural changes and thermal stability of charged $LiNi_xMn_yCo_zO_2$ cathode materials studied by combined in-situ time-resolved XRD and mass spectroscopy. *ACS Appl. Mater. Interfaces* **2014**, *6*, 22594–22601. [CrossRef]
8. Zheng, J.; Liu, T.; Hu, Z.; Wie, Y.; Song, X.; Ren, Y.; Wang, W.; Rao, M.; Lin, Y.; Chen, Z.; et al. Tuning of thermal stability in layered $Li(Ni_xMn_yCo_z)O_2$. *J. Am. Chem. Soc.* **2016**, *138*, 13326–13334. [CrossRef]
9. Tian, C.; Xu, Y.; KaN, W.; Sokaras, D.; Nordlund, D.; Shen, H.; Chen, K.; Liu, Y.; Doeff, M. Distinct surface and bulk thermal behaviors of $LiNi_{0.6}Mn_{0.2}Co_{0.2}O_2$ cathode materials as a function of state of charge. *ACS Appl. Mat. Interfaces* **2020**, *12*, 11643–11656. [CrossRef]
10. Ma, M.; Chernova, N.; Toby, B.; Zavalij, P.; Whittingham, M. Structural and electrochemical behavior of $LiMn_{0.4}Ni_{0.4}Co_{0.2}O_2$. *J. Power Sources* **2007**, *165*, 517–534. [CrossRef]
11. Cupid, D.M.; Reif, A.; Seifert, H.J. Enthalpy of formation of $Li_{1+x}Mn_{2-x}O_4$ (0<x<0.1) spinel phases. *Thermochim. Acta* **2015**, *599*, 35–41.
12. Ngala, K.; Chernova, N.A.; Ma, M.; Mamak, M.; Zavalija, P.Y.; Whittingham, M.S. The synthesis, characterization and electrochemical behavior of the layered $LiNi_{0.4}Mn_{0.4}Co_{0.2}O_2$ compound. *J. Mater. Chem.* **2004**, *14*, 214–220. [CrossRef]
13. Yin, S.-C.; Rho, Y.-H.; Swainson, I.; Nazar, L. X-ray/Neutron diffraction and electrochemical studies of Lithium de-/re-intercalation in $Li_{1-x}Co_{1/3}Ni_{1/3}Mn_{1/3}O_2$ (x=0–>1). *Chem. Mater.* **2006**, *18*, 1901–1910. [CrossRef]
14. Noh, H.; Youn, S.; Yoon, C.; Sun, Y. Comparison of the structural and electrochemical properties of layered $Li[Ni_xCo_yMn_z]O_2$ (x=1/3, 0.5, 0.6, 0.7, 0.8 and 0.85) cathode material for lithium-ion batteries. *J. Power Sources* **2013**, *233*, 121–130. [CrossRef]
15. Koyama, Y.; Tanaka, I.; Adachi, H.; Makimura, Y.; Ohzuku, T. Crystal and electronic structures of superstructural $Li_{1-x}[Co_{1/3}Ni_{1/3}Mn_{1/3}]O_2$ ($0 \leq x \leq 1$). *J. Power Sources* **2003**, *119*, 644–648. [CrossRef]
16. Kim, J.M.; Chung, H.T. The first cycle characteristics of $Li[Ni_{1/3}Co_{1/3}Mn_{1/3}]O_2$ charged up to 4.7 V. *Electrochim. Acta* **2004**, *49*, 937–944. [CrossRef]
17. Qiao, R.; Liu, J.; Kourtakis, K.; Roelofs, M.; Peterson, D.; Duff, J.; Deibler, D.; Wray, L.; Yang, W. Transition-metal redox evolution in $LiNi_{0.5}Mn_{0.3}Co_{0.2}O_2$ electrodes at high potentials. *J. Power Sources* **2017**, *360*, 294–300. [CrossRef]
18. Masoumi, M.; Cupid, D.; Reichmann, T.; Music, D.; Schneider, J.; Seifert, H. Enthalpies of formation of layered $LiNi_xMn_xCo_{1-2x}O_2$ compounds as promising Li-ion battery cathode materials. *Int. J. Mater. Res.* **2017**, *108*, 1–10. [CrossRef]
19. Wang, M.; Navrotsky, A. Enthalpy of formation of $LiNiO_2$, $LiCoO_2$ and their solid solution, $LiNi_{1-x}Co_xO_2$. *Solid State Ion.* **2004**, *166*, 167–173. [CrossRef]

20. Dinsdale, A.T. SGTE data for pure elements. *Calphad* **1991**, *15*, 317–425. [CrossRef]
21. Wang, M. Enthalpy of formation of Li_xCoO_2 ($0.5 \leq x \leq 1.0$). *J. Electrochem. Soc.* **2005**, *152*, J82–J84. [CrossRef]
22. Glushko, V.P.; Medvedev, V.A. *Thermal Constants of Substances*; Hemisphere Publishing Company: New York, NY, USA, 1990.
23. Wang, M.; Navrotsky, A. Thermochemistry of $Li_{1+x}Mn_{2-x}O_4$ ($0 \leq x \leq 1/3$) spinel. *J. Solid State Chem.* **2005**, *178*, 1182–1189. [CrossRef]

Disclaimer/Publisher's Note: The statements, opinions and data contained in all publications are solely those of the individual author(s) and contributor(s) and not of MDPI and/or the editor(s). MDPI and/or the editor(s) disclaim responsibility for any injury to people or property resulting from any ideas, methods, instructions or products referred to in the content.